Available online at www.sciencedirect.com
SCIENCE DIRECT®
Journal of Nuclear Materials 328 (2004) 11–20
journal of nuclear materials
www.elsevier.com/locate/jnucmat

Effect of prior thermal treatment on the microchemistry and crack propagation of proton-irradiated AISI 304 stainless steels

L.H. Wang [a,*], C.H. Tsai [b], J.J. Kai [b]

[a] *Materials Research Laboratories, Industrial Technology Research Institute, Building 52, 195-5 Chung-Hsing Road, Section 4, Chutung, Hsinchu 310, Taiwan*
[b] *National Tsin-Hua University, Hsinchu, Taiwan*

Received 25 August 2003; accepted 2 February 2004

Abstract

The effect of prior thermal treatment on crack growth was investigated on proton-irradiated Type 304 stainless steel (SS) of initially solution annealed (SA) and thermally sensitized (SEN) conditions. The Cr depletion profiles were measured by field emission gun transmission electron microscopy/energy dispersive spectroscopy (FEGTEM/EDS) in an attempt to correlate grain boundary chromium composition with the measured crack growth rate. The results showed that the crack growth of the 1-dpa-irradiated SEN 304SS is substantially higher than that of SA 304SS with the same irradiation dose. The unirradiated SEN material initially started with a shallow Cr depletion profile near grain boundary. After 1 dpa irradiation with proton, the Cr depletion profile becomes narrower and deeper. In contrast, the grain boundary Cr concentration in the SA specimen at the same irradiation dose was higher than that of the SEN specimen, mainly due to an initial Cr enriched condition. Consequently, the irradiated SEN specimen exhibited a higher degree of sensitization in electrochemical potentiokinetic reactivation test and faster crack growth rate in the stress corrosion crack test. The absence of irradiation enhanced crack growth in heavily thermal-sensitized 304SS is probably attributed to slower radiation-induced Cr depletion as a result of pre-existing thermally induced grain boundary Cr depletion. It is a clear indication that the inverse Kirkendall effect was hampered by the back diffusion of Cr due to initially depleted Cr concentration gradient near grain boundary.

PACS: 81.70.−q; 61.72.Mm; 64.75.+g; 25.40.Ep

1. Introduction

Austenitic stainless steels (SSs) have been widely used as nuclear structural materials for reactor coolant piping, valve bodies, and vessel internals. Intergranular stress corrosion cracking (IGSCC) in recirculation piping used to be a major problem for plant operation in the 1970s. The IGSCC mechanism has been clearly demonstrated to be the result of the thermal sensitization of austenitic SS containing high carbon by preferentially forming chromium carbide precipitates along the grain boundary, which in turn led to chromium depletion near the grain interface.

Austenitic SS materials used in vessel internal structures exposed to both high temperature water and neutron irradiation have been observed to have the crack tendency, known as irradiation-assisted stress corrosion cracking (IASCC) in recent years. The intergranular cracking morphology is similar in appearance to IGSCC. Radiation induced Cr depletion at grain boundary

* Corresponding author. Tel.: +886-3 5915259; fax: +886-3 5820001.
E-mail address: liwang@itri.org.tw (L.H. Wang).

0022-3115/$ - see front matter © 2004 Elsevier B.V. All rights reserved.
doi:10.1016/j.jnucmat.2004.02.003

has also been observed to have the similar Cr concentration profile of thermal sensitization, but the depletion was not resulted from carbide precipitation. Inverse Kirkendall diffusion is the likely radiation mechanism for chromium depletion in the absence of grain boundary carbide. Unequal rates of solute–vacancy diffusion cause inverse Kirkendall migration. It is generally recognized that radiation-induced segregation (RIS) [1–6], particularly chromium depletion or so-called radiation sensitization, plays an important role in initiating IASCC of austenitic SSs [7–9] in oxidizing environments.

In addition to chromium depletion occurred in thermally sensitized SS, chromium enrichment at grain boundaries has been detected in solution annealed austenitic SSs. Binding of Cr–vacancy complexes at solution annealing temperature allows migration of the complexes to grain boundaries during cooling stage, resulting in enriched Cr concentration at grain boundary. Both processes of solution annealed and sensitized thermal treatment can be found when constructing components in nuclear reactors. The solution annealing treatment is a common thermal practice for vessel internal base materials made of austenitic SS. The latter thermally sensitized treatment is likely to occur in the heat affected zone of most welded core internal structures.

Grain boundary chromium concentration strongly affects the cracking susceptibility of austenitic SS. The relationship between critical chromium concentration and IGSCC susceptibility has been well established for unirradiated SS. To a lesser extent, a weaker relationship between chromium concentration and IASCC susceptibility has also been found. Currently, the IASCC susceptibility was mostly indexed by percentage of intergranular cracking area or strain to failure measured in SSRT test, but rarely by crack growth measurement. Moreover, the study of the synthesis effect of prior thermal treatments and irradiation on the grain boundary microchemistry evolution and subsequent impact the SCC resistance remained relatively limited. Only some research were made to investigate thermally induced Cr enrichment and its effects on radiation induced sensitization [10,11], and a few papers tried to address the effect of thermally induced Cr depletion on radiation sensitization. It is therefore imperative to understand how prior thermal history affects grain boundary composition change during irradiation and how these changes affect the SCC susceptibility.

In the present work, the effect of prior thermal treatment on the microchemistry evolution and crack growth was investigated on proton-irradiated Type 304SS in initially solution annealed (SA) and thermally sensitized (SEN) C-ring stress corrosion tests in simulated boiling water reactor (BWR) environments. Proton irradiation was frequently used to simulate the neutron irradiation to evaluate the mechanical and chemical property changes in the commercial nuclear reactors. The advantages using proton irradiation include more accessibility to available source of proton irradiation, shorter irradiation time due to higher flux, and higher flexibility on adjusting controlling parameters such as energy, temperature and flux, etc. The crack advance was monitored using reversing DC potential drop techniques. The degree of sensitization was evaluated by the electrochemical potentiokinetic reactivation (EPR) method. The Cr depletion profiles were measured by field emission gun transmission electron microscopy/energy dispersive spectroscopy.

2. Experimental procedures

2.1. Test specimens and proton irradiation

Tests were performed on proton-irradiated Type 304SS C-ring specimens (Fig. 1) with initially SA and SEN heat treatments. The final heat treatment of solution-annealed condition was 3 min at 1100 °C, then water quench. The grain size was of 20–30 μm. The chemical composition of the 304SS is listed in Table 1. The sensitized heat treatment was conducted at 650 °C for 100 h. A notch of 1-mm depth was cut at the central region of the inner radius. The irradiated samples were prepared by bombarding the notched areas with 5 MeV protons, using a tandem accelerator, at 450 °C to the total doses of 0.1 and 1 dpa to simulate neutron irradiation at commercial BWRs [12]. The depth of irradiation damage region were calculated to be 80 μm using TRIM-95 code [13] as depicted in Fig. 2. The damage rate was estimated to be about 1×10^{-6} dpa/s at the examined region.

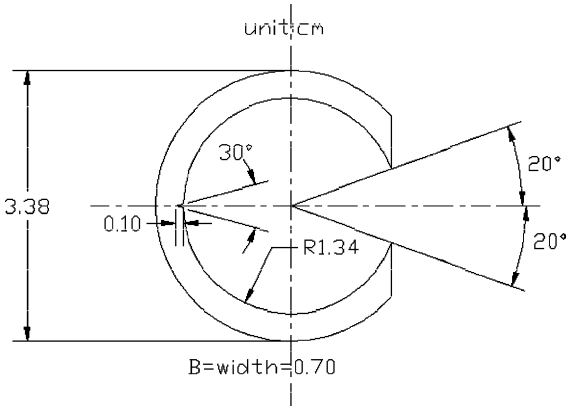

Fig. 1. Dimensions of the C-ring specimen.

Table 1
Chemical composition of the 304 stainless steel

	(wt%)									
	C	Si	Mn	P	S	Cr	Ni	Mo	N	Fe
304SS	0.047	0.50	1.49	0.025	0.002	18.04	8.23	0.036	0.056	bal

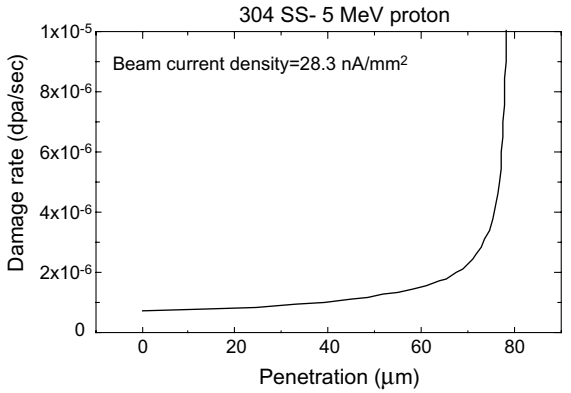

Fig. 2. Dpa Profile of 5 MeV H^+ penetrating into 304 stainless steel calculated from TRIM-95 code.

2.2. SCC tests

All stress corrosion–cracking (SCC) tests were conducted in high purity, oxygen-saturated water at 288 °C and 7.6 MPa. The inlet conductivity was maintained at 1 μS/cm with H_2SO_4 addition. The outlet conductivity remained almost at the same value as the inlet. The dissolved oxygen was controlled at 32 ppm by bubbling pure oxygen in feed water reservoir. Fig. 3 shows the schematic of the water circulation loop. The C-ring specimens were under the constant loading, exerted by the hydraulic pressure within the autoclave by pushing the pull rod outward. A load cell and LVDT were installed on the loading train to measure the applied load and the displacement. The applied stress intensity was 30 MPa $\sqrt{\text{m}}$, as calculated with the following equation [14].

$$K\ (\text{MPa}\sqrt{\text{m}}) = \frac{P}{Bw^{1/2}}\left(3\frac{r_1}{w} + 1.9 + 1.1\frac{a}{w}\right) \times \left[1 + 0.25\left(1 - \frac{a}{w}\right)^2\left(1 - \frac{r_1}{r_2}\right)\right] f\left(\frac{a}{w}\right), \quad (1)$$

$$f\left(\frac{a}{w}\right) = \left[\left(\frac{a}{w}\right)^{1/2} \Big/ \left(1 - \frac{a}{w}\right)^{3/2}\right] \times \left[3.74 - 6.3\left(\frac{a}{w}\right) + 6.32\left(\frac{a}{w}\right)^2 - 2.43\left(\frac{a}{w}\right)^3\right], \quad (2)$$

where K is the stress intensity factor; P, the load (kN); B, the width (cm); w, the wall thickness (cm); r_1, the inner radius (cm); r_2, the outer radius (cm); a, the crack length (cm).

Crack advance was monitored by a reversing direct current (RDC) potential drop technique, which

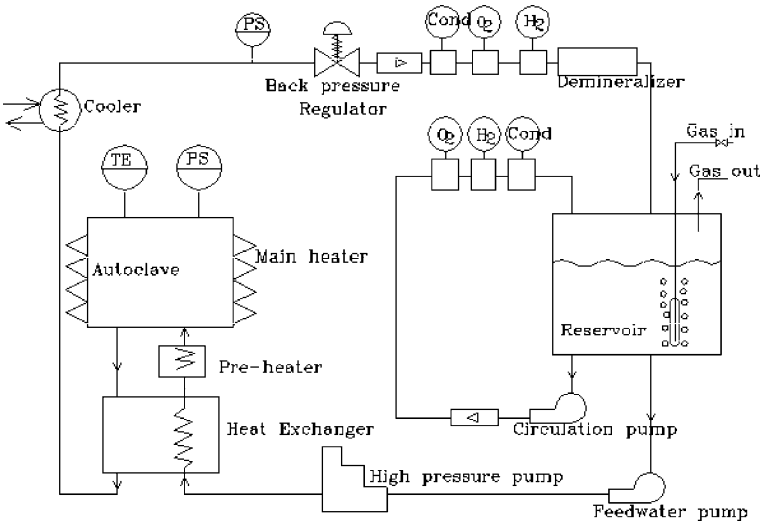

Fig. 3. Schematic of the water circulation loop.

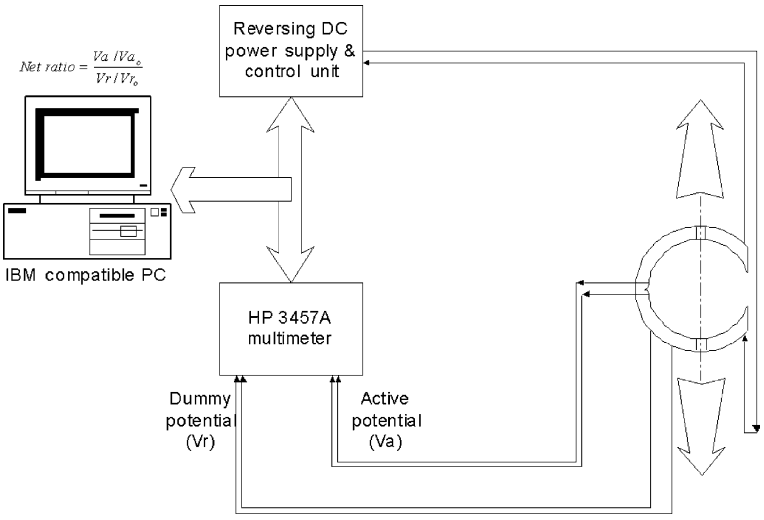

Fig. 4. Configuration of the RDC setup.

measured the crack length with a typical resolution of less than 5 μm. Platinum current and potential probe leads were attached on the C-ring specimens for DC potential drop measurements of crack length. During measurement, a 3 A current flowed through the sample to generate geometry dependent potential field. The direction of current flow was reversed about once per second to reduce measurement errors associated with thermocouple effects and current source offsets. Potential measurement data are averaged and stored in a hard disk file typically once every 150 s. The computer control of the current reversal, data acquisition, data averaging, the measuring instruments and the lead wire connection are shown schematically in Fig. 4. The conversion of RDC signal to crack length was made by comparing with the calibrated data from the air-fatigued crack growth test on specimen of identical geometry and with the crack growth depth observed by a scanning electron microscope (SEM). The crack growth rate was obtained only when the correlation coefficient of linear regression of the crack length vs. time data exceeded 0.9. Each crack length made from RDC conversion was later verified by microscopic measurement of fracture surface, and the accuracy has been shown to be typically within 5%.

2.3. EPR tests

The degree of sensitization of each specimen was evaluated with the single loop electrochemical potentiokinetic reactivation method. The proton-irradiation region was limited to a rectangular area of 10 mm × 20 mm. Two square samples of 5 × 5 mm located within the irradiated area were cut out to exclude the non-irradiated region. The sample with proton-irradiated surface exposed was mounted in the epoxy resin for subsequent EPR test. The testing environments were 0.5 M H_2SO_4 + 0.01 M KSCN at room temperature. The solution was deaerated by continuous nitrogen purging during the test. When the corrosion potential became stable, the specimen was first cathodically treated at −600 mV (vs. saturated calomel electrode, SCE) for 5 min. The potential was then raised stepwise to +200 mV (vs. SCE), held for 5 min to passivate the surface film, and reverse-scanned in the cathodic direction to −400 mV (vs. SCE) at 100 mV/min. EPR value in this paper was normalized by the specimen area and grain size following the method proposed by Clarke [15]. After the EPR test, the specimen surface characteristics were examined with an optical microscope (OM).

2.4. Grain boundary microchemistry measurements

After the SCC test, two thin sections were sectioned out from the inner surfaces of each C-ring specimen. Only the areas at 30 μm away from surface were selected for grain boundary microchemical analysis in order to avoid surface effects and the peak damage. The details on preparation of TEM specimens were described previously [16–18]. The observations of grain boundary segregation were performed on JEOL-2010F FEGTEM with LINK EDS. This instrument provides a small beam diameter of 0.5 nm with an acceleration voltage of 200 kV.

3. Results

Fig. 5 shows the crack growth measurements in unirradiated and irradiated 304SS with prior SA and SEN thermal treatments. Only the irradiated region, i.e.

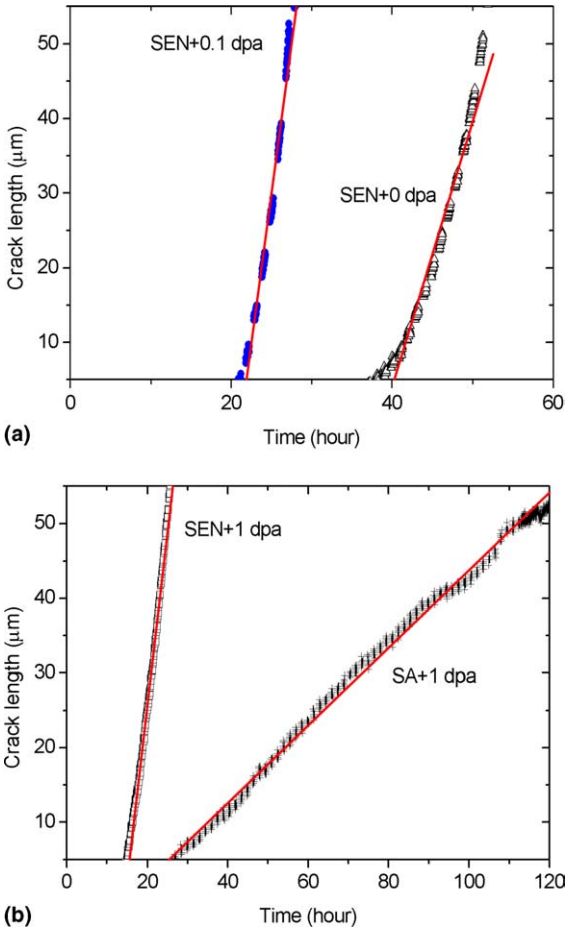

Fig. 5. Typical examples of crack growth measurements of (a) SEN and SEN + 0.1 dpa 304SS (b) SEN + 1 dpa and SA + 1 dpa 304SS.

80 μm below surface, was taken into consideration for determining the crack growth rate (CGR). The irradiated region contained roughly two to three grains in this sample of 20–30 μm grain size. The testing sample was specifically avoided any solution annealing and thus preserve as-received condition to assure adequate grain size and crack growth requirements. The crack growth rates as a function of the dpa value are summarized in Fig. 6. The unirradiated SA 304SS did not crack after long test duration of 1013 h. For comparison purpose, it was marked by a very low crack growth rate with a downward arrow. From the results in Fig. 6, radiation enhancement on the crack growth rates of SA 304SS is clearly observed. As for SEN 304SS samples, radiation only slightly increases the crack growth rate, although the irradiation dose did not correlate so well with the crack growth rate in sensitized samples. The enhancement factor on the crack growth rate is higher of SA 304SS than SEN 304SS. However, the crack growth of

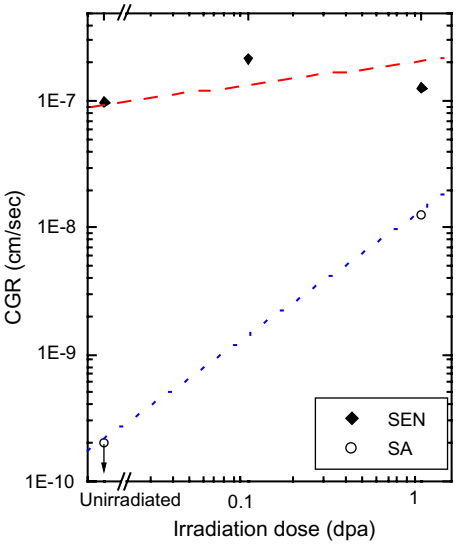

Fig. 6. Summary of the crack growth rates in function of the dpa values.

the 1-dpa-irradiated SEN 304SS is substantially higher than that of SA 304SS with the same irradiation dose. The vast different crack growth rates exhibited by samples of SEN and SA 304SS with same irradiation dose clearly illustrated that the prior thermal treatments could significantly affect the CGRs in these proton-irradiated materials. The morphology of cracks revealed by SEM is all intergranular cracking, as depicted in Fig. 7.

Fig. 8 summarizes the results of EPR tests on the SEN and SA specimens in both irradiated and unirradiated conditions. The EPR results clearly show there are two groups of curves. The SEN specimens exhibited higher corrosion current. The corrosion currents of SA specimens are substantially lower, even with 1 dpa irradiation. The observations under OM showed that the grain boundaries of SEN specimens were etched, whereas the SA specimens exhibited no grain boundary etching. Small numbers of etching pits were observed in both materials. That means the corrosion currents flowed not only from grain boundary areas, but also from intragranular pits. Therefore, the real EPR values should be lower than the values calculated based on the measured corrosion currents. The normalized EPR value against dpa was shown in Fig. 9.

The Cr distributions at grain boundaries measured by FEGTEM/EDS were plotted in Fig. 10(a) for the unirradiated and irradiated SEN 304SS. The wider and shallower Cr depletion profile with triangular points is characteristic of the unirradiated SEN material. The width (full width half maximum) of the Cr concentration profiles lie between 100 and 150 nm. After 1 dpa irradiation with proton, the Cr depletion profile becomes narrower and steeper. The average Cr concentration at

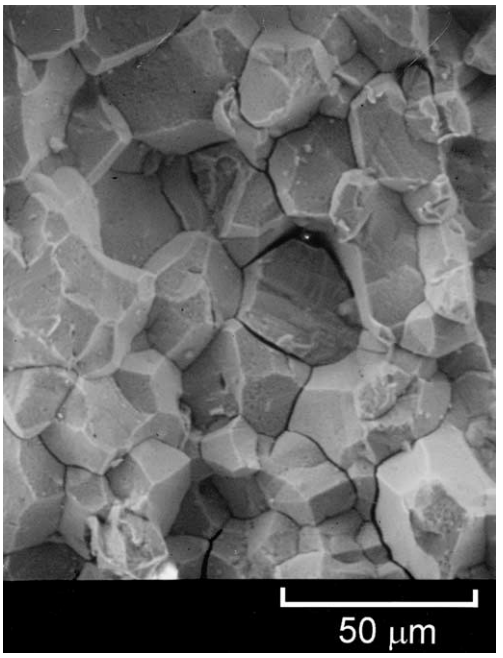

Fig. 7. Crack morphology in SEN + 1 dpa 304SS revealed by SEM is intergranular cracking.

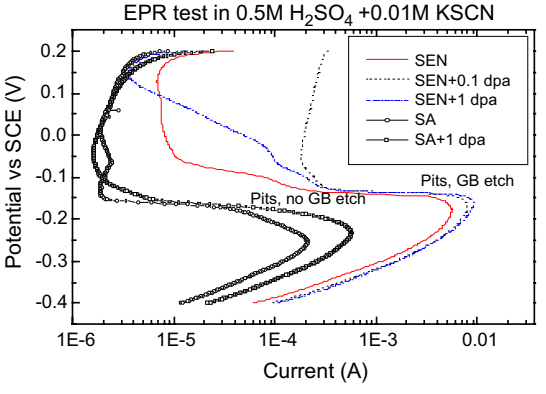

Fig. 8. Results of EPR tests on both the initially SEN and SA specimens.

the grain boundary for the 1-dpa-irradiated SEN SS decreased to about 11.5 at.%, which is 2.5 at.% lower than pre-irradiated condition. Fig. 10(b) depicts the grain boundary Cr distributions of the unirradiated and 1-dpa-irradiated SA 304SS. An initial Cr enriched condition was observed in the sample of unirradiated SA 304SS. After 1 dpa proton irradiation, the average Cr concentration at the grain boundary decreased to about 16.4 at.%. The grain boundary Cr concentration in the SA specimen was higher than the SEN specimen after 1 dpa irradiation.

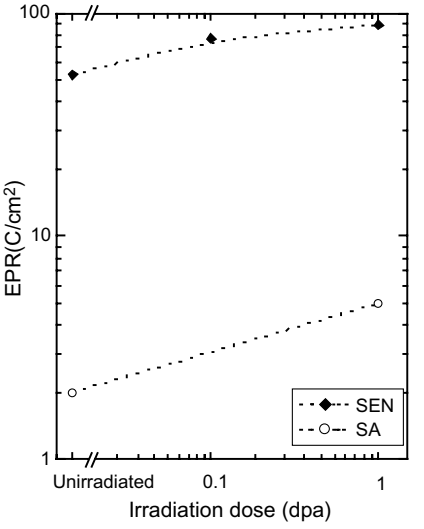

Fig. 9. Normalized EPR value against dpa.

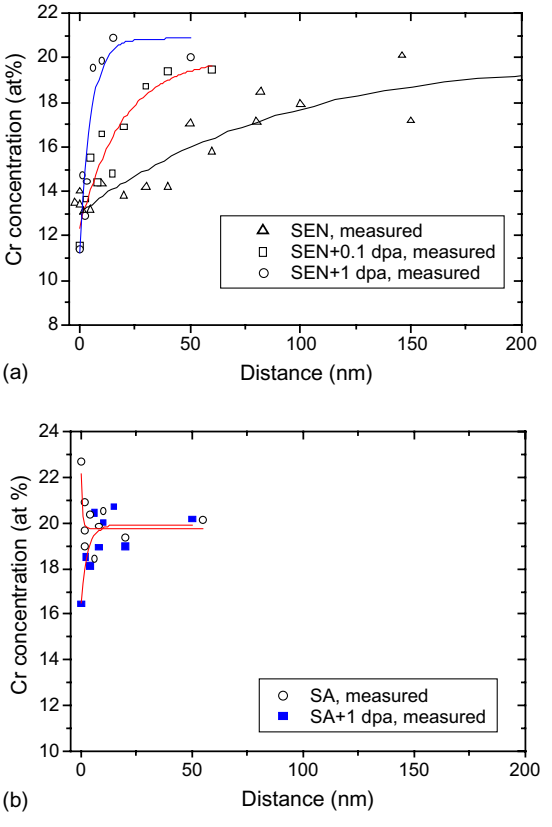

Fig. 10. The grain boundary Cr distribution of the unirradiated and irradiated (a) SEN 304SS and (b) SA 304SS.

4. Discussion

Prior thermal history significantly changed the degree of sensitization of irradiated 304SS as shown in Fig. 9, and affected the crack growth rate as depicted in Fig. 6. The EPR results in Fig. 9 showed higher degree of sensitization (DOS) in irradiated 304SS with prior SEN treatment, and lower degree of sensitization in irradiated 304SS with SA treatment. The similar trend was found in crack growth data as depicted in Fig. 6. By comparing Fig. 6 with Fig. 9, the result implied that the crack growth rate might be related with degree of sensitization regardless whether the DOS was resulted from different irradiation dose or dissimilar prior thermal treatment. Fig. 11 describes the relationship between the crack growth rates and EPR values and clearly shows that the CGRs can be reasonably correlated to the EPR values, although the relation is not perfectly linear. This plot indicates that the CGR is low for low DOS material, and higher for materials with medium to high DOS. The CGR gradually approached a plateau as EPR value reached high DOS. The EPR value can be treated as a qualitative indicator to evaluate the crack growth rate of proton-irradiated SS304 with different prior thermal treatments.

The concentration profiles measured by STEM/EDS provide a direct evidence to illustrate that the vast differences of degree of sensitization of SEN and SA 304SS under the same irradiation dose. The unirradiated SEN material started with an initial Cr depletion profile near grain boundary. After 1 dpa irradiation with proton, the Cr depletion profile becomes narrower and steeper. By comparing the grain boundary Cr concentrations from samples of unirradiated, 0.1 and 1 dpa, it can be shown that grain boundary Cr content tends to be lower as radiation dose increases.

The grain boundary Cr concentration of irradiated SA specimen was not as low as that of the SEN specimen, mainly due to an initial Cr enriched condition. Consequently, the irradiated SEN specimen showed higher DOS in EPR test and higher crack growth rate in the SCC test. In other words, the prior thermal history could significantly affect the subsequent evolution of radiation sensitization. Similar degree of proton irradiation could lead to widely varying Cr distribution, DOS, and crack growth rate for 304SS undergoing different pre-existing thermal treatments.

Fig. 12 describes the crack growth rate with the Cr concentration at grain boundary for unirradiated and irradiated SA and SEN samples. The intergranular crack growth rate of proton-irradiated SS with various prior thermal history exhibited the same linear correlation with the Cr concentration at grain boundary, although two curves are needed to illustrate the relationship between crack growth rate and dpa for different prior thermal history. Bruemmer et al. [4] compared the relationship between Cr depletion and IGSCC susceptibility of unirradiated and irradiated SSs, and found that as the grain boundary Cr concentration drops below 16–17 wt% for 304SS, stainless steels become susceptible to intergranular cracking under oxidizing water environments with slow strain rate test (SSRT). The IGSCC susceptibility was indexed by percentage of intergranular cracking area or strain to failure measured in SSRT test. In our study, crack growth rate drops as the grain

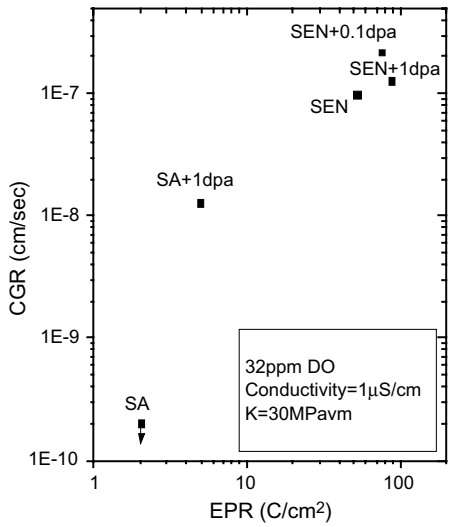

Fig. 11. Plot of the crack growth rate against EPR values. It clearly showed that the CGRs were reasonably correlated to the EPR values.

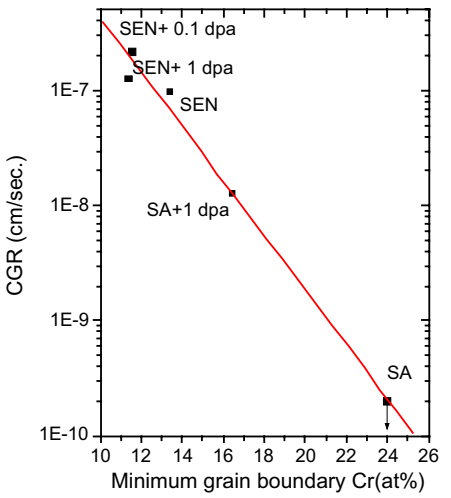

Fig. 12. Correlation of the measured intergranular crack growth rates in function of the minimum grain boundary Cr concentration in the proton irradiated SSs.

boundary Cr concentration increases. However, the threshold grain boundary Cr concentration for cessation of intergranular crack cannot be concluded in this test, because limited data measured in the region of lower crack growth rate.

It is generally agreed that there exists a threshold fluence for IASCC to occur [19]. The threshold value is somewhat lower in BWR (5×10^{24} n/m^2, $E>1$ MeV) than in pressurized water reactor ($1–2\times10^{25}$ n/m^2, $E>0.1$ MeV) environments. The consensus was based on the direct observations from SSRT data and limited field experiences of vessel internal cracks. However, the prior thermal histories will influence the SCC resistance, and therefore change the threshold neutron fluence of SCC initiation. Andresen [20] summarized the data of Jacobs and Kodama, and found the onset fluence of SCC shifted to higher value on irradiated 304/316SS with initial grain boundary Cr enrichment. Kodama et al. [21] observed that intergranular cracking scarcely occurs, which indicates good IASCC resistance in the materials of 304/316SS each having large pre-irradiation Cr enrichment even under the irradiation fluence up to about 2×10^{25} n/m^2 in BWR environments. However, Onchi et al. [22] tested the irradiated thermally sensitized SS, but found that the SCC occurred even with the neutron fluence down to 5×10^{22} n/m^2. If only the effect of radiation fluence on crack growth rate were considered, it would be difficult to explain the large variation of crack growth rates of irradiated specimens. The grain boundary Cr content tends to be lower as radiation dose increases, whereas the grain boundary Cr content of SA specimens is higher than that of the sample with prior sensitization treatment. The delay of Cr depletion in SA samples is probably due to initial Cr enriched distribution. Therefore, the prior SEN thermal treatment aggravates the SCC in the irradiated 304SS to occur, but the prior SA thermal treatment alleviates the SCC to occur.

To examine the effects of prior thermal treatment on the radiation induced Cr decrement ($\Delta Cr = Cr - Cr_{ini}$), the Cr decrements were plotted against irradiation doses in Fig. 13. It is found that the Cr decrement ($\Delta Cr = 2.5$ at.%, from 14 to 11.5 at.%) in SEN SS is less than that ($\Delta Cr = 6.6$ at.%, from 23 to 16.4 at.%) in SA SS, as radiation dose reaches to 1 dpa. The difference may be attributed to the reverse Cr flux of pre-existing concentration gradient. Radiation sensitization is created due to a non-equilibrium process in which solute atoms interact with radiation induced vacancies and interstitial. Nickel atoms that diffuse more slowly become enriched near grain boundary and chromium atoms with higher diffusion rate become depleted. This phenomenon is known as inverse Kirkendall effect. The flux of solute atom k to grain boundary can be described by the following equation [23,24],

$$\Omega J_k = -D_k\alpha\nabla C_k + d_{kv}C_k\nabla C_v - d_{ki}C_k\nabla C_i, \qquad (3)$$

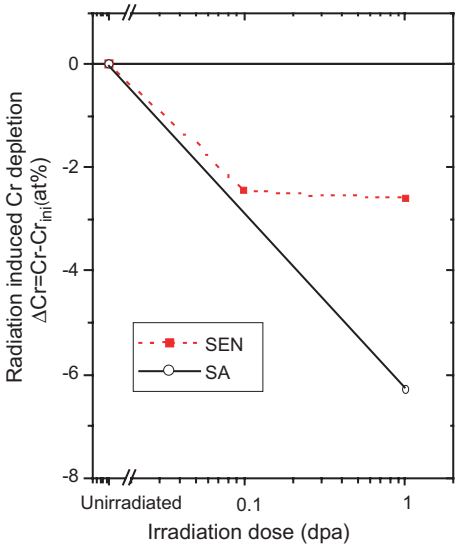

Fig. 13. Effects of prior thermal treatment on the radiation induced Cr decrement.

where Ω = atomic volume, $D_k = d_{kv}C_v + d_{ki}C_i$, d_{kj} = diffusivity of k atom via j defect, α = thermodynamic factor.

The solute atom flux includes concentration gradient flux (the first term in Eq. (3)) and inverse Kirkendall flux (the last two terms in Eq. (3)). As the specimen has pre-existing Cr depletion profile due to thermal sensitization, the reverse concentration gradient flux will balance off some inverse Kirkendall flux, and thus impede the Cr depletion. However, the prior enriched Cr concentration will accelerate the Cr diffusion flux away from grain boundary. This could explain that, as depicted in Fig. 13, the Cr depletion was enhanced by irradiation when initial grain boundary Cr concentration was enriched before irradiation (e.g. SA condition), but radiation induced Cr decrement developed more slowly if the initial Cr concentration was depleted (e.g. SEN condition). Similar observations can also be found in Okada's work [25] for the heavily sensitized 304SS. Although the lower grain boundary Cr concentration of irradiated SEN sample is superimposed by the initial thermally sensitized Cr concentration and the following radiation induced Cr depletion, the Cr depletion was indeed hampered by the reverse Cr flow that back diffused from the initially thermally sensitized Cr concentration gradient. The hampered Cr depletion probably explained that additional irradiation doses will not further increase the crack growth rate and cause only minor variation in the EPR values of SEN materials under irradiation.

Fig. 14 depicts the degree of sensitization in terms of EPR value (EPR-DOS) vs. measured Cr concentration at grain boundary. The EPR-DOS value appeared strongly correlated with the grain boundary Cr content,

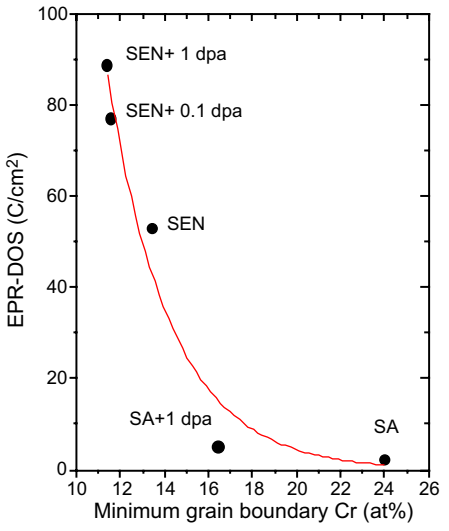

Fig. 14. Degree of sensitization vs. grain boundary Cr concentration.

regardless of the sensitization from thermal, irradiation, or combined effect of thermal and radiation sensitization. When the Cr concentration at grain boundary decreases below 16 at.% (~15 wt% in this study), larger EPR-DOS value is expected, although Bruemmer et al. [26] observed that the EPR test attacks regions below ~13.5 wt%.

5. Conclusions

(1) Prior thermal treatment significantly affected the degree of sensitization of irradiated 304SS, and consequently influenced the crack growth rate.

(2) The DOS and CGR of the 1-dpa-irradiated thermally sensitized 304SS is substantially higher than solution annealed 304SS with the same irradiation dose. The lower grain boundary Cr content of the 1-dpa-irradiated thermally sensitized 304SS caused the higher DOS and CGR.

(3) The Cr depletion was enhanced by irradiation when initial grain boundary Cr concentration was enriched before irradiation (in SA condition), but radiation induced Cr decrement developed more slowly if the initial Cr concentration was depleted (in SEN condition).

(4) The intergranular crack growth rate of proton-irradiated SS correlates linearly with the Cr concentration at grain boundary regardless of its prior thermal or irradiation histories.

(5) The EPR value can be treated as a qualitative indicator to evaluate the crack growth rate of proton-irradiated SS304 with different prior thermal treatments.

Acknowledgements

The authors are grateful to the kind assistance of Nuclear Science and Technology Development Center – National Tsin-Hua University on the proton irradiation and to Dr F.R. Chen and Dr T.S. Duh for the FEG-TEM/EDS work. This study was sponsored by the Taiwan Power Company. The work on RIS model calculation was financially supported by the National Science Council of the Republic of China under contract number: NSC85-2212-E007-011 and NSC86-2212-E007-051.

References

[1] A.J. Jacobs, in: Effects of Radiation on Materials: 16th International Symposium, ASTM STP 1175, ASTM, Philadelphia, January, 1994, p. 902.
[2] M. Kodama, R. Katsura, J. Morisawa, S. Nishimura, S. Suzuki, K. Asano, K. Fukuya, K. Nakata, in: Proc. of Sixth International Symposium on Environmental Degradation of Materials in Nuclear Power Systems – Water Reactors, San Diego, California, 1–5 August 1993, The Minerals, Metals and Materials Society (TMS), Warrendale, PA, 1993, p. 583.
[3] K. Asano, K. Fukuya, K. Nakata, M. Kodama, in: Proc. of 5th International Symposium on Environmental Degradation of Materials in Nuclear Power Systems – Water Reactors Monterey, California, 25–29 August 1991, American Nuclear Society (ANS), La Grange Park, IL, 1992, p. 838.
[4] S.M. Bruemmer, B.W. Arey, L.A. Charlot, in: Proc. of 6th International Symposium on Environmental Degradation of Materials in Nuclear Power Systems – Water Reactors, San Diego, California, 1–5 August 1993, The Minerals, Metals and Materials Society (TMS), Warrendale, PA, 1993, p. 277.
[5] D.L. Damcott, T.L. Allen, G.S. Was, J. Nucl. Mater. 225 (1995) 97.
[6] S. Watanabe, N. Sakaguchi, N. Hashimoto, H. Takahashi, J. Nucl. Mater. 224 (1995) 158.
[7] S. Kasahara, K. Nakata, K. Fukuya, S. Shima, A.J. Jacobs, G.P. Wozadlo, S. Suzuki, in: Proc. of 6th International Symposium on Environmental Degradation of Materials in Nuclear Power Systems – Water Reactors, San Diego, California, 1–5 August 1993, The Minerals, Metals and Materials Society (TMS), Warrendale, PA, 1993, p. 615.
[8] A.J. Jacobs, G.P. Wozadlo, K. Nakata, S. Kasahara, T. Okada, S. Kawano, S. Suzuki, in: Proc. of 6th International Symposium on Environmental Degradation of Materials in Nuclear Power Systems – Water Reactors, San Diego, California, 1–5 August 1993, The Minerals, Metals and Materials Society (TMS), Warrendale, PA, 1993, p. 597.
[9] M. Kodama, K. Fukuya, H. Kayano, in: Effects of Radiation on Materials: 16th International Symposium, ASTM STP 1175, ASTM, Philadelphia, January, 1994, p. 889.
[10] E.P. Simonen, S.M. Bruemmer, in: Proc. of the 8th International Symposium on Environmental Degradation

of Materials in Nuclear Power Systems – Water Reactors, Amelia Island, Florida, 10–14 August 1997, American Nuclear Society (ANS), La Grange Park, IL, 1997, p. 751.
[11] E.P. Simonen, S.M. Bruemmer, Corrosion/1998, San Diego, California, 22–27 March 1998, NACE International, Houston, TX, 1998, paper no. 139.
[12] G.S. Was, T.R. Allen, J.T. Busby, J. Gan, D. Damcott, D. Carter, M Atzmon, in: Microstructural Processes in Irradiated Materials of Materials Research Society Symposium Proceeding Volume 540, 30 November–2 December 1998, The Materials Research Society, Warrendale, PA, 1999, p. 421.
[13] J.P. Biersack, L.G. Haggmark, Nucl. Instrum. and Meth. 174 (1980) 257.
[14] Richard W. Hertzberg, Deformation and Fracture Mechanics of Engineering Materials, John Wiley, New York, 1989, p. 656.
[15] W.L. Clarke, The EPR method for the detection of sensitization in stainless steels, US Nuclear Regulatory Commission, Washington, DC, NUREG/CR-1095, February 1981.
[16] J.J. Kai, L.H. Wang, T.S. Duh, F.R. Chen, C. Fong, in: Proc. of the 8th International Symposium on Environmental Degradation of Materials in Nuclear Power Systems – Water Reactors, Amelia Island, Florida, 10–14 August 1997, American Nuclear Society (ANS), La Grange Park, IL, 1997, p. 766.
[17] T.S. Duh, J.J. Kai, F.R. Chen, L.H. Wang, J. Nucl. Mater. 258–263 (1998) 2064.
[18] T.S. Duh, J.J. Kai, F.R. Chen, J. Nucl. Mater. 283–287 (2000) 198.
[19] P.L. Andresen, in: R.H. Jones (Ed.), Stress Corrosion Cracking – Material Performance and Evaluation, ASM, 1992, p. 181.
[20] P.L. Andresen, in: Proc. of 7th International Symposium on Environmental Degradation of Materials in Nuclear Power Systems – Water Reactors, Breckenridge, Colorado, 7–10 August 1995, NACE International, Houston, TX, 1995, p. 893.
[21] M. Kodama, Y. Ishiyama, S. Namatame, S. Suzuki, K. Fukuya, H. Sakamoto, K. Nakata, T. Kato, in: Proc. of 9th International Symposium on Environmental Degradation of Materials in Nuclear Power Systems – Water Reactors, Newport Beach, California, 1–5 August 1999, The Minerals, Metals and Materials Society (TMS), Warrendale, PA, 1999, p. 923.
[22] T. Onchi, K. Hide, M. Mayuzumi, K. Dohi, T. Niiho, Corrosion 53 (1997) 778.
[23] L.H. Wang, C.H. Tsai, J.J. Kai, T.S. Duh, Microstructural Processes in Irradiated Materials of Materials Research Society Symposium Proceeding Volume 540, 30 November–2 December 1998, The Materials Research Society, Warrendale, PA, 1999, p. 489.
[24] G.S. Was, T. Allen, J. Nucl. Mater. 205 (1993) 332.
[25] O. Okada, K. Nakata, S. Kasahara, T. Aoyama, in: Proc. of the 8th International Symposium on Environmental Degradation of Materials in Nuclear Power Systems – Water Reactors, Amelia Island, Florida, 10–14 August 1997, American Nuclear Society (ANS), La Grange Park, IL, 1997, p. 743.
[26] S.M. Bruemmer, L.A. Charlot, B.W. Arey, Corrosion 44 (1988) 328.